Optical probes and techniques for molecular contrast enhancement in coherence imaging

Stephen A. Boppart
Amy L. Oldenburg
Chenyang Xu
Daniel L. Marks
University of Illinois at Urbana-Champaign
Biophotonics Imaging Laboratory
Beckman Institute for Advanced Science and Technology
Department of Electrical and Computer Engineering
Department of Bioengineering
Colleges of Engineering and Medicine
Urbana, Illinois 61801
E-mail: boppart@uiuc.edu

Abstract. Optics has played a key role in the rapidly developing field of molecular imaging. The spectroscopic nature and high-resolution imaging capabilities of light provide a means for probing biological morphology and function at the cellular and molecular levels. While the use of bioluminescent and fluorescent probes has become a mainstay in optical molecular imaging, a large number of other optical imaging modalities exist that can be included in this emerging field. *In vivo* imaging technologies such as optical coherence tomography and reflectance confocal microscopy have had limited use of molecular probes. In the last few years, novel nonfluorescent and nonbioluminescent molecular imaging probes have been developed that will initiate new directions in coherent optical molecular imaging. Classes of probes reviewed in this work include those that alter the local optical scattering or absorption properties of the tissue, those that modulate these local optical properties in a predictable manner, and those that are detected utilizing spectroscopic optical coherence tomography (OCT) principles. In addition to spectroscopic OCT, novel nonlinear interferometric imaging techniques have recently been developed to detect endogenous molecules. Probes and techniques designed for coherent molecular imaging are likely to improve the detection and diagnostic capabilities of OCT. [DOI: 10.1117/1.2008974]

Keywords: molecular imaging; contrast agents; optical coherence tomography; scattering; absorption; nonlinear optics.

Paper 05071 SSR received Mar. 18, 2005; revised manuscript received May 3, 2005; accepted for publication May 5, 2005; published online Aug. 15, 2005.

1 Introduction

The trend in biomedical imaging is toward early detection and diagnosis of disease. Since virtually all disease originates at the molecular and cellular level, detection and imaging systems with resolutions and sensitivities capable of imaging at these levels would be most suitable. As such, optics has played a central role, providing not only sufficient resolution to resolve morphological features at the cellular level, but also wavelength sensitivity, which enables the detection and localization of the optical signal from spectroscopically specific endogenous molecules, transfected genetic sequences, or exogenous molecules or probes. The mere presence of spectroscopically identifiable probes, however, has limited informational content unless the presence can be linked to some physiologically or functionally meaningful parameter. By functionalizing and targeting probes to specific cellular and molecular sites, the detection and spatial localization of the probes through imaging techniques add molecular specificity. The potential of molecular optical imaging therefore becomes great, providing morphological, spatial, and functional information at the molecular level.

While one may consider the historical and present use of stains and dyes in histology as a form of molecularly specific targeting with subsequent optical imaging, the field of molecular imaging has traditionally been defined as the detection of a molecularly specific signal, either from a targeted exogenous agent or some endogenous molecule, in a living organism. Under this definition, optical molecular imaging is still in its infancy but is rapidly expanding in scope through the use of new exogenous molecular probes and through the development of novel techniques for the detection of endogenous molecules. Figure 1 metaphorically diagrams the plethora of molecular probes, emitted optical signals, optical detection methods, and applications of optical molecular imaging. Numerous research studies have demonstrated the use of fluorescent markers tagged to a wide variety of specific cell receptors.[1–3] The use of bioluminescent probes (luciferases) demonstrated optical molecular imaging in small animal models, primarily mice, and enabled the noninvasive detection of disease and tracking of progression in a wide range of pathologies and processes, including infection,[4,5] cancer,[6,7] and stem cell fates.[8] The advancement of highly sensitive detection systems and cooled CCD cameras has permitted detection of extremely weak fluorescent and bioluminescent signals originating deep within highly scattering tissues.[9] Recent ef-

Address all correspondence to Stephen A. Boppart, Dept. of Electrical Engineering, Univ. of Illinois/Urbana-Champaign, Beckman Institute, 405 N. Mathews Ave., Urbana, IL 61801. Tel: 217–244–7479. Fax: 217–244–1995. E-mail: boppart@uiuc.edu

1083-3668/2005/10(4)/041208/14/$22.00 © 2005 SPIE

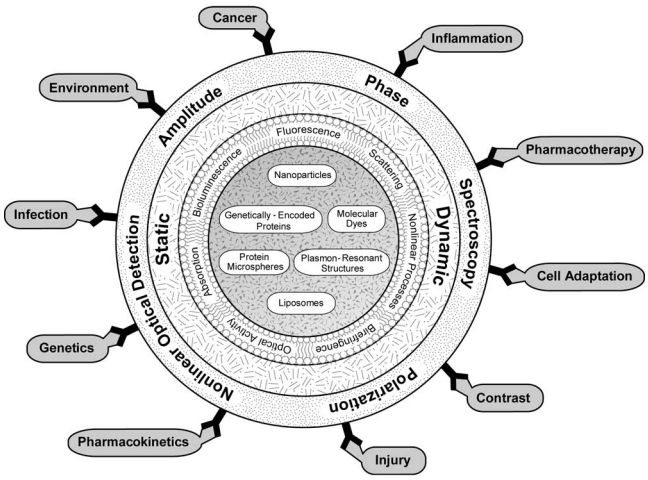

Fig. 1 Metaphorical diagram of the wide spectrum of optical molecular probes, their optical signals, their optical detection parameters, and their applications. In addition to fluorescent and bioluminescent probes, a diverse number of other probes and techniques comprise optical molecular imaging, including those detected and imaged with coherent light.

forts in the design of bioluminescent and fluorescent probes have been to extend the absorption and emission spectra of these probes into the near-infrared, where absorption and scattering can be minimized and depth of excitation and detection of emission can be maximized.[10,11]

The majority of optical probes developed in recent years have been based on the emission of a bioluminescent or fluorescent signal. While these methods now have an established track record of use, there remains a number of other optical imaging methods that would equally benefit from novel optical probes to not only nonspecifically enhance contrast within images, but ultimately provide the same molecular specificity afforded by the bioluminescent and fluorescent probes (Fig. 1). A number of nonfluorescent detection and imaging techniques include *in vivo* video (white) light microscopy, reflectance confocal microscopy, and coherence imaging techniques such as optical coherence tomography (OCT).

OCT is an emerging biomedical imaging technology that is based on the detection of backreflected signals using low-coherence interferometry and optical ranging within tissues.[12–14] Because it senses elastically scattered light which maintains the coherence of the incident light, OCT is not capable of directly detecting bioluminescent or fluorescent signals. Despite the rapid development, application, and integration of OCT into the biological sciences, medicine, and surgery over the last decade, there has been little prior development and no regular use of contrast agents or molecular probes designed specifically for this modality. Early applications of OCT focused on the morphological imaging capabilities of this technology.[15–20] In recent years, attention has been given to the use of functional OCT techniques such as Doppler OCT,[21–25] polarization-sensitive OCT,[26–29] and the detection of functional electrical activity in neural tissue,[30–32] which provides additional information based on optical changes that correspond to physiological parameters. The coherence-imaging capabilities of OCT offer numerous advantages over fluorescence- and bioluminescence-based techniques, including heterodyne detection to improve signal to noise, and the ability to extract phase information from the detected signal, which permits velocimetric (Doppler) and spectroscopic imaging. With the advent of molecular contrast methods and molecular OCT imaging techniques,[33] by way of the use of exogenous probes or contrast agents, or by the use of novel techniques to detect endogenous molecules, the imaging and diagnostic capabilities of OCT have the potential to be extended dramatically.

Currently, new methods and classes of optical probes are being developed to enhance OCT contrast in unique ways, with the goal of enabling molecular OCT imaging. This work reviews the current research efforts in this area and describes future directions. While the majority of these research and development efforts have been directed toward OCT, similar probes and methodologies are applicable to other nonfluorescent optical imaging techniques, including reflectance confocal and white-light microscopy.

2 Probes for Coherence Imaging

While the majority of molecularly targeted probes are based on fluorescence or bioluminescence, optical imaging technologies insensitive to inelastically scattered light must rely on other fundamental changes in optical properties, namely changes in scattering, absorption, polarization, or a time- or frequency-dependent modulation of amplitude, phase, or frequency of the light. Next, several classes of these probes are discussed.

2.1 *Scattering Probes*

Probes designed for efficient light scattering are sensed either directly by detecting their scattered light or indirectly through their attenuation of the incident light. Imaging modalities such as OCT are based on detecting backscattering and operate in the "biological window" of near-infrared wavelengths where absorption is minimal and attenuation is governed primarily by scattering. To alter the intensity of backscattered light in OCT, scattering probes must introduce a local region of index of refraction change. For instance, even the introduction of air into tissue produces a significant change in index, thereby increasing the intensity of the backscattered light in OCT. One of the first demonstrations of scattering probes was the use of gold nanoparticles in electron microscopy to label specific regions within cells.[34] Commercially available air-filled (Albunex®) and perfluorocarbon-filled albumin microspheres for use as contrast-enhancing agents in ultrasound[35] were also used to enhance optical contrast in OCT.[36] With recent advances in sonochemistry and chemical modification of probes, a wide variety of engineered microspheres have been fabricated to optimize the optical scattering properties of these probes (Fig. 2 and Table 1).[37] Scattering microspheres were fabricated using a high-frequency ultrasound probe placed at the interface between liquids where high-energy ultrasound waves produce cavitation and microsphere formation. Microspheres 500 nm to 15 μm in diameter could be fabricated by varying the energy used during sonication. This fabrication protocol enables a wide range of flexibility in combining core, shell, and surface composition as listed in Table 1. Since scattering increases with the magnitude of the refractive index change, the use of metals or other materials with an index

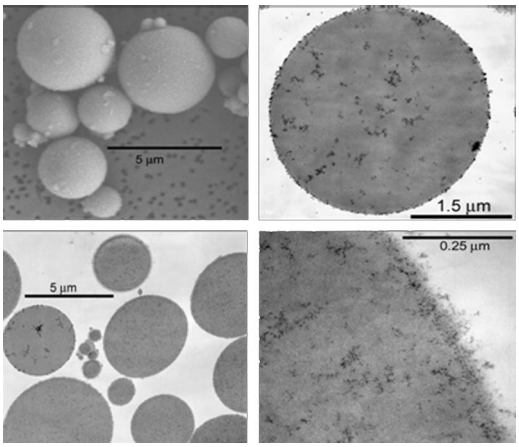

Fig. 2 Microsphere contrast agents with nanoparticle surface, shell, and core modifications. Scanning and transmission electron micrographs of protein microspheres encapsulating an iron-oxide colloid suspension in an oil core are shown. Flexible microsphere fabrication parameters enable not only variation in size, but also core, shell, and surface composition as listed in Table 1.

significantly different from tissue is desirable. Quantitative analysis of optical absorption and scattering properties of engineered microspheres have demonstrated that the use of highly scattering nanoparticles of gold, melanin, carbon, and iron oxide produce strong scattering in OCT (Fig. 2).[37]

These engineered protein microspheres have been demonstrated in *in vivo* OCT imaging in animal models. Figure 3 shows representative images of exposed mouse liver before and after the tail-vein injection of gold-coated protein microspheres.[37] The administration of the nontargeted scattering microspheres increased the scattering from the liver, while revealing low signal from the liver vasculature. The primary mechanism of uptake in the liver was via phagocytosis by the resident macrophages (Kuppfer cells). Scanning electron micrographs of macrophages (Fig. 3) with and without exposure

Table 1 Engineered microsphere core, shell, and surface combinations.

Protein shells	*Inner cores*	*Surface modifications*
Albumin	Air, O_2, N_2, Ar	PEG
Hemoglobin	Vegetable oils	Fluorescein
Pepsin	Water	Iron oxide colloid
Immunoglobulins	Organic liquids	Immunoglobulins
Lipase	Acetoacetate	Folate
Peroxidases	Fluorocarbons	Gd complexes
Modified myoglobin	Iodinated agents	Monoclonal antibodies
	Gd complexes	Gold
	Ferrofluids	Carbon
		Melanin

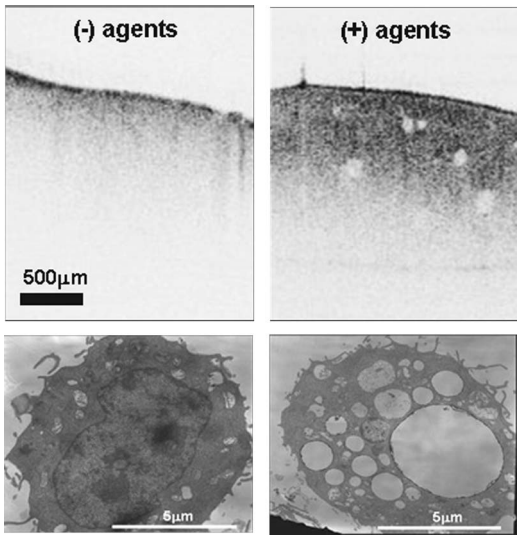

Fig. 3 Protein microspheres as OCT contrast agents. Top set: OCT images of an *in vivo* mouse liver before and after tail-vein injection of gold-coated protein microspheres. Postadministration of the contrast agents reveal increased scattering from the liver, where Kuppfer cells had phagocytosed the scattering microspheres. The low-scattering regions are likely the liver vasculature. Bottom set: Scanning electron micrographs of cultured macrophages without (lower left) and with (lower right) exposure to microspheres. The large circular-appearing cavities represent cross sections of phagocytosed microspheres. Modified figure reprinted with permission.[37]

to microspheres show clearly that the microspheres are readily phagocytosed and broken down within these cells. Early *in vitro* cell viability studies have shown that these engineered microspheres have little to no cellular toxicity.[38]

The administration of these engineered microspheres does provide dynamic scattering changes within tissue. Following mouse tail-vein injection of iron-oxide encapsulated microspheres, transient regional scattering changes were observed while imaging the exposed mouse intestinal wall (Fig. 4). Scattering variations were noted around a vascular region, while minimal changes were observed in an avascular region immediately after the administration of the agents. While the larger microspheres are likely to remain in the vascular system due to their size, it remains to be determined if the observed scattering changes were due to extravasation of smaller microspheres, degraded microsphere fragments, or a local accumulation of microspheres within the vascular system.

In addition to the flexibility of altering the scattering properties (and equally the absorption properties) of these microspheres, the potential exists for these probes to be highly multifunctional. The protein-based shell of these microspheres is readily functionalized, as has been demonstrated in ultrasound imaging.[39] With the increasing number of viable molecular targets available, such as the overexpression of cell-surface receptors in disease states like cancer, it will be possible to similarly target these microspheres to molecularly specific sites. The physical size of these microspheres (2 to 5 μm average) prohibits their use as an agent that will extravasate from the intravascular space into the extravascular and extracellular spaces for cell-specific targeting. Their use as a blood pool agent would be feasible for defining vascular networks,

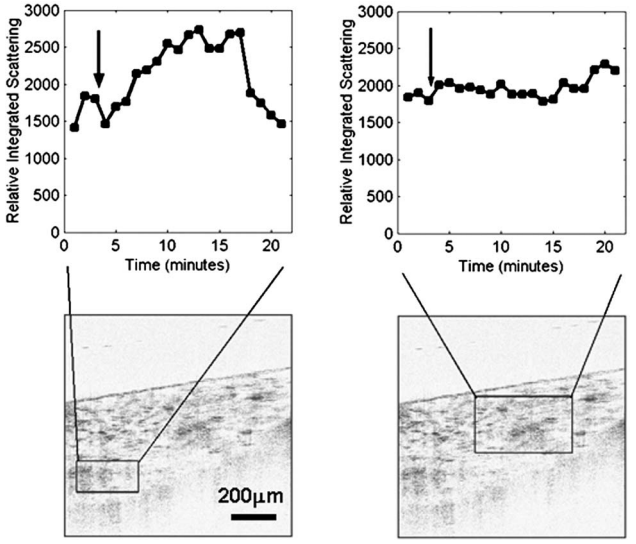

Fig. 4 Dynamic scattering changes in tissue. Scattering changes within OCT images are noted following tail-vein injection of iron-oxide encapsulated microspheres. OCT images were acquired from the exposed mouse intestinal wall at locations corresponding to vascular (left column) and avascular (right column) regions. The arrows indicate the time of contrast agent injection.

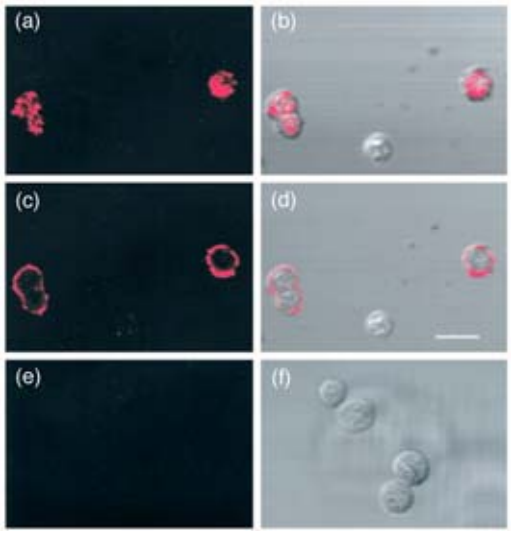

Fig. 5 Reflectance confocal microscopy images of SiHa cells labeled with anti-EGFR/gold conjugates. Laser scanning confocal reflectance images (left) are superimposed over confocal transmittance images (right). The scattering from the gold is false-colorized as red. Targeted agent binding is shown in (a) through (d) compared to nonspecific binding shown in (e) and (f). The scale bar is ~30 μm. Figure reprinted with permission.[40]

identifying regions of altered perfusion, or for labeling regions of vessels expressing specific markers during diseases such as angiogenesis and atherosclerosis. However, their relatively large size is fortuitous as a drug delivery vehicle by encapsulating drugs that can be delivered to specific sites. The engineered scattering microsphere enables the fabrication of a scattering probe that uses selected nanoparticles spatially oriented on the microsphere shell, or within the core material to optimize the scattering cross section, whereby the use of nanoparticles alone, although smaller in size, is not likely to alter the local scattering property of the tissue as strongly.

The use of scattering nanoparticles alone, without attachment to larger microspheres, would be preferred for their small size, their ready ability to extravasate outside of the vascular system, and the potential to be directed toward individual cells. The highly scattering (plasmon-resonant) nature of gold nanoparticles was used to label individual cells expressing specific cell-surface receptors.[40,41] Gold nanoparticles were conjugated to an anti-epithelium growth factor receptor (EGFR) and incubated with SiHa cells (Fig. 5). These highly scattering gold nanoparticles, depending on their size, aggregation, and local environment, potentially exhibit surface plasmon resonances, which are an additional class of OCT contrast agents discussed in a later section. When viewed with reflectance confocal microscopy and compared to transmission-mode microscopy, site-specific contrast enhancement was observed.

2.2 *Modulating Probes*

In OCT, sensing a change in local scattering induced by a probe is frequently plagued by speckle and background scattering from the tissue medium. Higher probe imaging specificity may be achieved by modifying an observable property of the probe *in situ* while leaving the background tissue unperturbed. Modulation and subsequent filtering of the signal results in background rejection of unperturbed tissue structures, analogous to the background reduction leveraged by the use of fluorescent probes. Recently, optical contrast agents with modulatable fluorescence have been developed that enable the rejection of stationary background signals. Fluorescent microspheres with a ferromagnetic core were coated on one hemisphere with a metal, then magnetized. The microspheres were rotated using a rotating magnetic field, resulting in modulation of their fluorescence emission.[42] The magnetically induced blinking drastically improved the detection sensitivity of these agents in fluorescence microscopy. For OCT, modulating probes have been investigated primarily along two channels: modifiable scattering using magnetic particles, and modifiable absorption using dye molecules. Discussion of the latter is postponed to the following section on absorbing probes.

The use of particles with high magnetic susceptibility and/or ferromagnetic property is highly desirable, because tissue exhibits no ferromagnetism and only weak magnetic susceptibility ($\chi < 10^{-5}$). Iron oxide such as magnetite ($\chi \sim 1$) is a good candidate due to its known biocompatibility after polymer coating. In the presence of a high magnetic field gradient, particles with high magnetic susceptibility embedded in tissue experience a gradient force, and ferromagnetic particles rotate to align their internal magnetization along the field.[43] The resulting magnetomotion of the particle and perturbation of the surrounding cells and organelles result in a change in the local scattering (Fig. 6, top panels). In an elastic medium, the particle returns to its original position and orientation after removal of the magnetic field. This permits modulation of its position by repetitively modifying the magnetic field (by toggling it on and off in the examples discussed here). Modulation at any frequency outside the bandwidth of the OCT back-

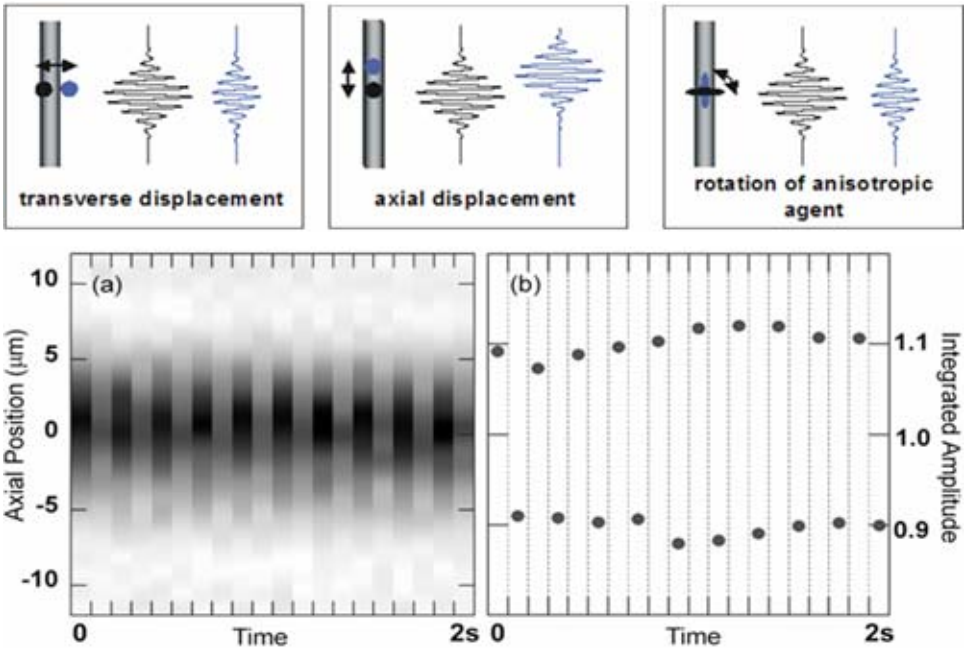

Fig. 6 Magnetomotive OCT principle. Top panels: Perturbation of magnetic particles within the OCT imaging light beam and the subsequent change in the OCT interferogram are illustrated. Magnetomotive contrast may be obtained via transverse or axial displacement, or by rotation of an anisotropic particle. Bottom panels: (a) repetitive axial scans at 10 Hz of a magnetite microparticle embedded within 5% agarose gel during magnetic field modulation. Each axial scan was acquired with the magnetic field alternately on and off. (b) Integrated demodulated OCT signal amplitude for each axial scan in (a) resulting in 20% signal modulation. Magnetically induced displacement of the optically scattering magnetic particle and subsequent restoration by the agarose medium accounts for the observed regularity in the modulation of the optical scattering. Figures reprinted with permission.[44,46]

scattering signal allows differentiation of tissue structure from magnetic particles.[44] In practice, this has been performed by toggling power to an electromagnet between each successive axial OCT scan (Fig. 6, bottom panels), or by modulating the power several times during acquisition of each pixel and using lock-in detection.[45]

In a recent study,[46] macrophage cell labeling in tissue scaffolds using magnetic markers and magnetomotive OCT was demonstrated (Fig. 7). The ability to detect magnetic particles attached to cells and inside highly scattering media such as chicken skin (Fig. 8) suggests future potential for this technique *in vivo*. A promising avenue of probe development is protein microspheres that incorporate iron-oxide nanoparticles either as an encapsulated ferrofluid or embedded into the protein shell (Fig. 2). Recent advances in biomedicine that utilize superparamagnetic and ferromagnetic particles, such as for hyperthermic therapy,[47] magnetorelaxometry,[48] magnetic drug targeting,[49] and magnetic resonance (MR) molecular contrast imaging,[50] suggest a wide array of possible translational applications in conjunction with magnetomotive OCT. Of particular interest is the development of multimodal targeted magnetic probes, which are identified at the mesoscopic scale using magnetic resonance imaging (MRI) and subsequently localized at the microscopic scale using high-resolution, small field-of-view techniques such as OCT to provide intraoperative surgical guidance.

2.3 *Absorbing Probes*

The use of absorbing probes for OCT is based on the regional attenuation due to the absorption. For homogeneous tissue, this regional attenuation can be detected as the reduced backscattering intensity in the deeper structures. However, because biological tissue is inhomogeneous, the scattering efficiency varies considerably for different layers. The detection of absorbing probes based on intensity attenuation alone is usually not accurate. Therefore, spectrally uniform absorbing agents, such as ink or broadband dye, have little value in OCT. However, two approaches can drastically improve the detection accuracy. The first approach is to utilize the fact that some absorbing probes absorb light differently for different wavelengths. Spectroscopic analysis of the light affected by these probes can drastically improve the detection accuracy. An intuitive way to understand this is to consider the less absorbing frequency bands as the built-in control for the more absorbing frequency bands. Hence, the difference in tissue scattering efficiency can be normalized to some degree. The second approach utilizes absorbers that have modifiable absorption in the presence of optical pumping. By turning the optical pumping on or off, background rejection can be achieved through differencing of pairs of images obtained while the agent property was changed. Examples of the two approaches will be described in this section. A more detailed description of spectroscopic OCT (SOCT) measurement techniques and algorithms, which can be used to detect absorbing probes, is presented in a later section.

Within the broadband laser spectra offered by state-of-the-art femtosecond titanium:sapphire lasers (centered at 800 nm), none of the major molecular components of tissue, namely water, structural proteins without chromophores, most carbohydrates, lipids, and nucleic acids, are spectrally active.

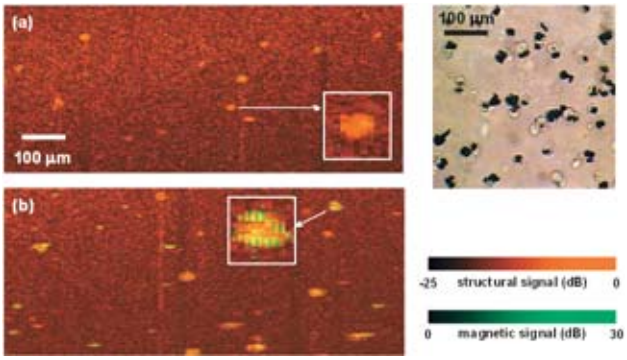

Fig. 7 Magnetomotive OCT for labeling and tracking single cells. Representative images of macrophage cells in a 3-D scaffold displaying structural OCT (red) and magnetomotive OCT (green) signals as indicated by color bar scales representing the dynamic ranges within the image. (a) Control macrophages and (b) macrophages allowed to uptake magnetite microparticles. Insets are 40×40 μm. Apparent cell sizes ($\sim$8 to 30 μm) are consistent with light microscopy observations as shown. Figure reprinted with permission.[46]

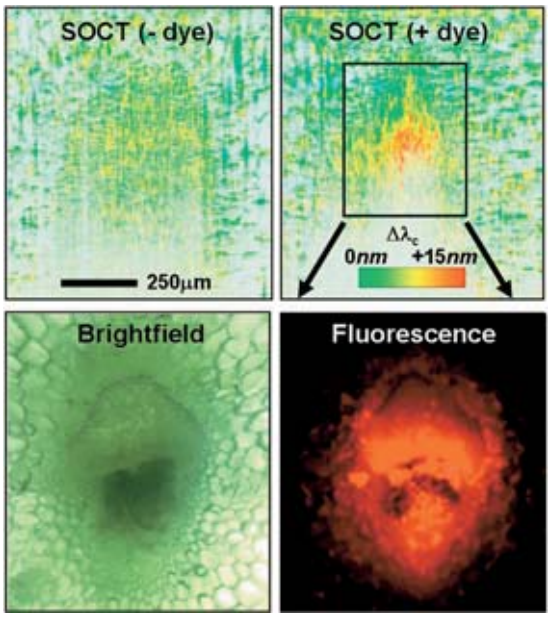

Fig. 9 Near-infrared dye contrast enhancement in SOCT. Cross sectional SOCT images of a celery stalk without and with NIR dye present within the vascular bundle (top left and right, respectively). The color bar shows correspondence between pseudocolor labeling and spectral centroid shift in the image. Corresponding brightfield light microscopy and fluorescence microscopy show the vascular bundle and the surrounding collenchyma tissue (bottom left and right, respectively). Figure reprinted with permission.[54]

For this reason, anatomical and biochemical research using SOCT to date has been limited to a few types of naturally occurring NIR absorbers such as deoxy- and oxy-hemoglobin (Hb/HbO_2) and melanin, with studies done *in vitro*.[51] This situation is very similar to conventional light microscopy imaging, where most tissue structures are colorless without the use of specific stains. It is therefore intuitive that "spectro-

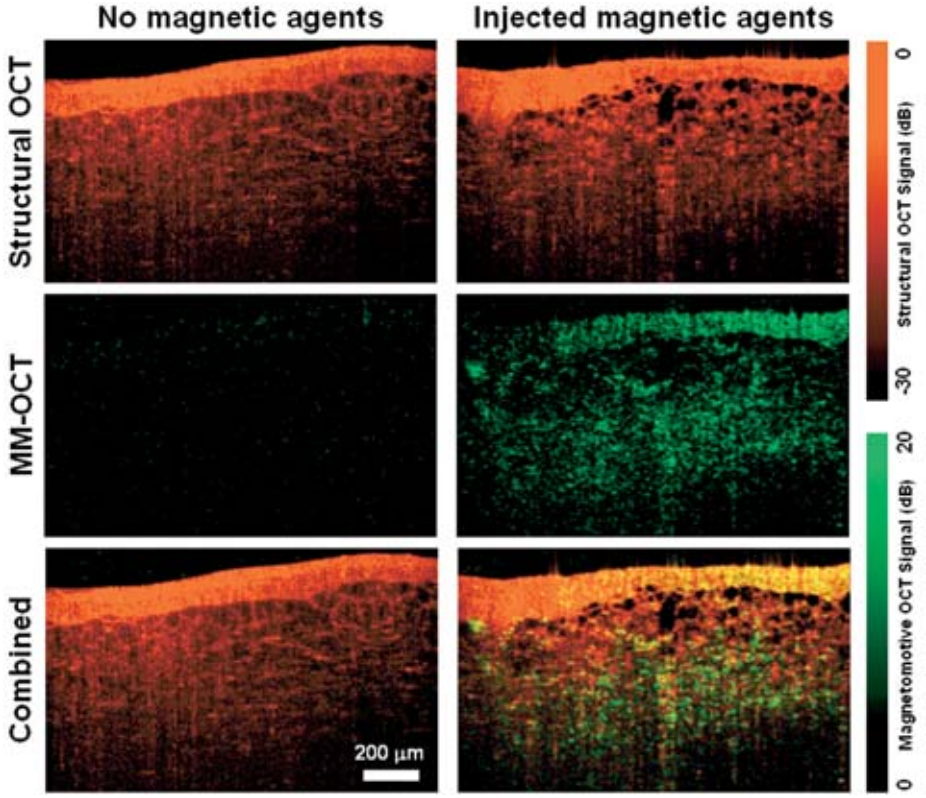

Fig. 8 Magnetomotive OCT in tissue. Images were acquired from *in vitro* chicken breast tissue. Structural and magnetomotive OCT images were acquired in tandem, without and with the topical administration of iron-oxide nanoparticles. Note the large dynamic range and excellent background signal rejection of this technique.

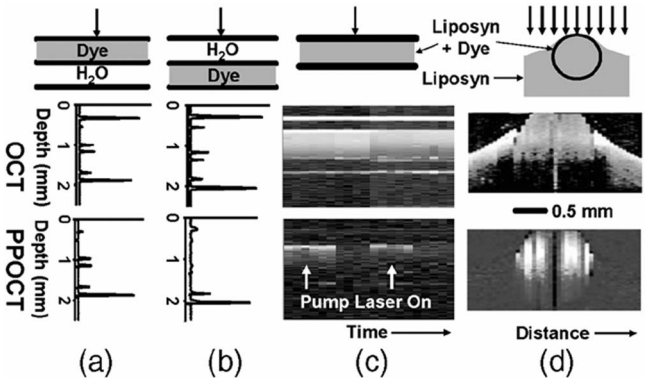

Fig. 10 Pump-probe OCT of phantoms with methylene blue dye in water. (a) and (b) A-scans of two-layer phantoms containing pure water and ~0.5-mM methylene blue dye in water at two different locations. (c) OCT and pump-probe-OCT M-mode scans of a single layer of ~0.5-mM methylene blue dye in 0.5% scattering Liposyn, with the pump laser alternatively on and off. (d) OCT and pump-probe-OCT images of a capillary tube filled with ~0.5-mM methylene dye in 0.5% scattering Liposyn. The pump-probe-OCT image reveals signal only from the dye region. Figure reprinted with permission.[55]

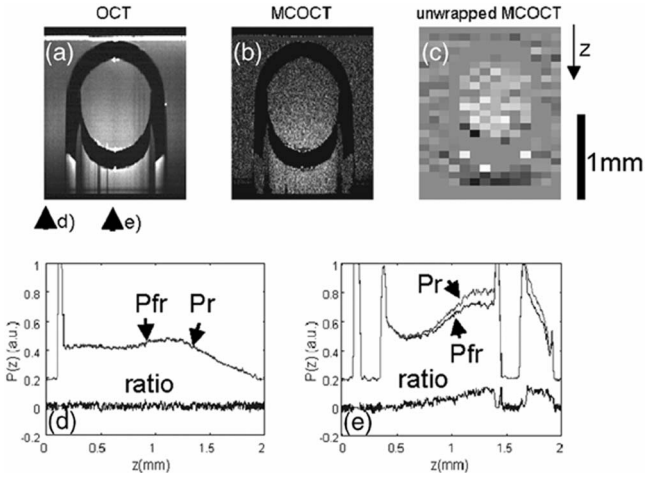

Fig. 11 Protein-based molecular-contrast OCT. (a) OCT image of phytochrome A in the Pr state. (b) Differential scan showing molecular-contrast regions of the phytochrome. (c) Unwrapped molecular-contrast-OCT image with the strongest signal originating from the region corresponding to the phytochrome protein. (d) A-scans through the medium (no phytochrome) in the Pr and Pfr states at the location indicated by the arrow in (a). (e) A-scans through the capillary tube containing the phytochrome in the Pr and Pfr states, extracted from the location indicated in (a). Figure reprinted with permission.[56]

scopic staining," with the use of dyes that are spectrally active in the NIR region, will enhance contrast in SOCT and potentially aid in differentiating tissue structures.

The simplest spectroscopic absorbing probes are the NIR dyes;[1,3,52] however, plasmon-resonant nanoparticles are also strongly absorbing in the NIR, with tunable peak absorption spectra and bandwidth. To facilitate spectroscopic OCT detection, it is desirable for NIR dyes or plasmon-resonant nanoparticles to have sharp, distinct, and stable absorption peaks within the OCT laser spectrum for more accurate labeling. Many commercially available fluorescence dyes, laser dyes, and optimized plasmon-resonant nanoparticles (spheres, shells, rods, cages) can be used for this purpose. In one example, the Federal Drug Administration (FDA)-approved NIR dye indocyanine green (ICG) has an absorption peak in 780 nm and a full width at half maximum (FWHM) of 70 nm, and was used in several studies.[53] While ICG has an absorption peak near the center wavelength of the Ti:sapphire laser spectrum, it is frequently advantageous to have an absorber that has an absorption peak off-center to enhance the spectroscopic contrast and the OCT imaging depth. For example, in a recent study, a NIR dye with strong absorption over the shorter half of the laser spectrum was used (Fig. 9). SOCT analysis was able to localize the dye distribution in the vascular system of a botanical specimen.[54]

The first experimentally demonstrated molecule with modifiable absorption in OCT was methylene blue,[55] which can be excited from its ground state (absorption peak at 650 nm) to its excited state (absorption peak at 830 nm) by using 650-nm optical excitation. Therefore, by switching optical excitation on and off, the absorption property at 830 can be modulated (Fig. 10). Because methylene blue has a rather short excitation state lifetime, a high pumping intensity was required. Other molecules with more stable excited molecular states were investigated to reduce the requirement in the pumping power. Phytochrome A, a naturally occurring plant protein with two distinct states of different absorption, was identified as a potential agent because one of its peak absorption states is in the commonly used OCT spectral range of the Ti:sapphire laser, and has very long transition durations on the order of a second (Fig. 11).[56]

2.4 *Plasmon-Resonant Probes*

Because Rayleigh scattering theory predicts that the scattering cross section scales as the sixth power of the particle diameter, it becomes increasingly difficult to achieve smaller, nanosize probes with sufficient cross section to be detected with OCT at concentrations that are nontoxic. To overcome this limitation, there has been extensive interest in the use of metal nanoparticles that exhibit a collective excitation of electrons at a characteristic light frequency, a property called the surface plasmon resonance (SPR).[57] At optical wavelengths, this is primarily observable in silver and gold, the latter being particularly useful in the near-infrared. A variety of SPR nanoparticle geometries are currently under investigation as optical probes, including nanospheres,[58] nanoshells,[59] nanorods,[60] and nanocages.[61] Because the resonance frequency is governed by particle geometry and the response exhibits an extremely narrow spectral linewidth, the possibility exists for multichannel imaging using an array of multitargeted probes whose resonance frequency is associated with a specific cell receptor.[62] However, the linewidth is often limited in practice by the ability to synthesize batches that are extremely monodisperse in size, and for gold nanoshells, other physical limitations to the linewidth have also been identified.[63] Recently, gold nanoparticles targeted against the epidermal growth factor receptor (EGFR) have been used as highly scattering agents for molecular sensitivity with structured illumination light microscopy.[64] Similarly, SPR nanoparticles are of interest in OCT because their small size en-

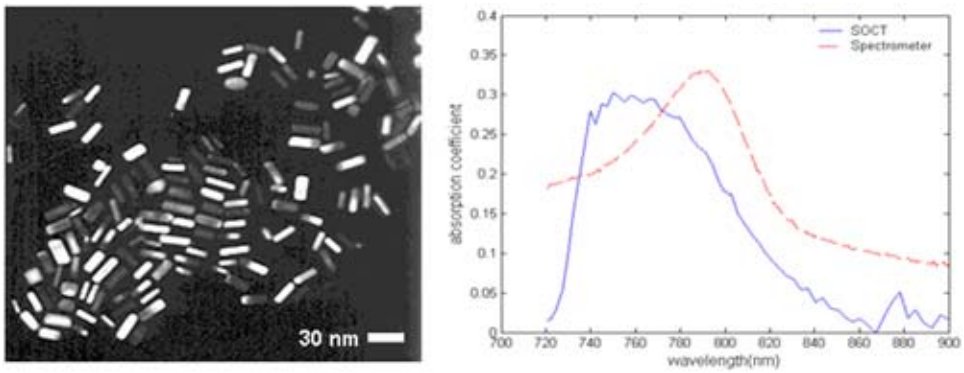

Fig. 12 Plasmon-resonant nanorods as absorbing OCT contrast agents. Scanning electron micrograph of nanorods, approximately 10×30 nm in size (left). Extinction spectrum of a solution of nanorods measured with a spectrometer and extracted from an OCT image using spectroscopic OCT algorithms (right). Spectroscopic OCT images of nanorods in solution show a red color-shift with increasing depth, corresponding to an increasing red-shift of the SOCT-extracted spectral centroid due to nanorods absorption.

ables extravasation from circulation into the extravascular space.

Plasmon-resonant nanoshell probes consist of a metal shell (Ag or Au) grown over a solid dielectric core (typically SiO_2). This geometry increases the magnitude of the local electromagnetic field at the nanoparticle surface, resulting in measured field enhancements of 10^6 and an implied enhancement of 10^{12} (Ref. 65). The resonance frequency is tuned by adjusting the core/shell size ratio,[66] and the albedo (relative contribution of scattering compared to absorption) is also variable based on particle geometry and can be tailored to match the application.[59] Highly scattering nanoshells labeled with the HER-2 antibody have been shown to target breast cancer cells as imaged with darkfield microscopy,[59] and also display a detectible signal when imaged with OCT. In a separate application, absorbing nanoshells increase photodamage induced by NIR illumination, as shown in an animal tumor model.[67]

Rod-shaped gold nanoparticles known as nanorods [Fig. 12(a)] are of considerable interest due to their unique spectral response consisting of a transverse plasmon resonance and a longer wavelength longitudinal plasmon resonance. The center wavelength of the longitudinal plasmon resonance increases nearly linearly with the aspect ratio of the rod,[68] and reaches near-infrared wavelengths with easily achieved aspect ratios greater than 3:1. Because nanorods with typical dimensions less than 80 nm are primarily absorbers,[60,69] they are detectible by OCT through their depth-dependent attenuation, resulting in a sensitivity of 25 μg/mL of nanorods (15×45 nm) within a tissue-like scattering solution.[60] This sensitivity is expected to increase with the use of spectroscopic-specific detection as described earlier. In particular, nanorods with a longitudinal plasmon resonance tuned to 780 nm and a narrow linewidth of ~50 nm have been detected with an OCT system utilizing a Ti:sapphire source (Fig. 12). SOCT has been able to extract the absorption spectra of these nanorods with good agreement to spectrometer measurements. The presence of these nanorods results in attenuation of approximately half the OCT incident light bandwidth and a depth-dependent shift of the backscattered light spectrum. Another intriguing nanoparticle geometry is that of the nanocage,[61] essentially a hollowed gold cube with porous walls, which, for nominal dimensions of 40 nm, exhibits a SPR near 800 nm. These nanocages are also primarily absorbers, and OCT imaging demonstrates detection at 1 nM in tissue phantoms. Bioconjugation of nanocages to HER-2 and specificity to breast cancer cells [visualized by scanning electron microscope (SEM)] has also been demonstrated.[61] It should also be noted that, to date, both nanocages and nanorods are significantly smaller than the nanoshells (~120 nm) currently used for OCT imaging. Further studies are required to determine what specific role the size of these nanoparticles plays in allowing them to extravasate out of the vasculature and into the extravascular space for *in vivo* cell targeting.

In conclusion, SPR particles afford a large optical cross section while maintaining a small physical size to enable high tissue mobility. Future work to improve the sensitivity of OCT to SPR particles may include polarization-sensitive detection of anisotropic particles, or coupling the particles with a magnetic domain to allow *in situ* modulation. The current state of the art includes the ability to separately target, image, and photothermally damage cancerous cells, suggesting that it may not be far in the future when each of these goals is obtained simultaneously using a single probe platform.

3 Molecular OCT Imaging of Endogenous Molecules

The previous methods of contrast in OCT depend on introducing an exogenous contrast agent into the tissue. Exogenous agents must be biocompatible, produce a sufficiently strong scattering or absorption signature to be detectable, and be specific to a molecular or cellular feature of interest. An alternate approach is to use the molecules of interest themselves as contrast agents, so that no foreign agents or probes need to be introduced. There are a number of molecular OCT imaging techniques that generate contrast from endogenous molecules present in the specimen. It should also be noted that the techniques discussed in the section could also be coupled with exogenous probes that may contain a more specific signature.

3.1 *Spectroscopic Optical Coherence Tomography*

Spectroscopic OCT analyzes not only the intensity, but also the spectrum of backscattered light in a spatially resolved manner. SOCT techniques are possible largely because OCT

utilizes broadband laser sources. Hence, the spectroscopic features within the laser spectrum can be detected. SOCT techniques are algorithmic, do not require special OCT imaging hardware, and can be implemented using either a time-domain or a spectral-domain OCT system.[70–72] Because the spectra of backscattered light are depth varying along the imaging axis, SOCT signals are nonstationary, with both time (depth) and frequency (wavelength) variations. Therefore, the central signal-processing step in SOCT analysis is to obtain the time-frequency analysis from the time-dependent interferogram signal (for a time-domain OCT system), or the frequency-dependent interferogram signal (for a spectral-domain OCT system). From the time-frequency analysis, different tissue properties can be retrieved.

The time-frequency analysis of the SOCT signal suffers the so-called time-frequency "uncertainty principle," which states that there exists an inherent tradeoff between spectral resolution and time (spatial) resolution.[73] Improvement in one implies degradation in the other. Early SOCT studies used linear time-frequency analysis methods such as the short time Fourier transform (STFT) and the wavelet transform.[70] Different time resolution and frequency resolution can be achieved by using time windows of different length (or wavelets of different scaling). In an effort to improve the joint time-frequency resolution, higher order transformations, such as the Wigner's distribution, can be used.[74] In general, it was determined that different SOCT imaging scenarios require different optimal time-frequency analysis methods.[73] For instance, the Cohen's-class time-frequency analysis generates the most compact time-frequency analysis, while linear time-frequency analysis offers the most reliable time-frequency analysis.[75] In both cases, if some prior information is known about the tissue, the molecules of interest, or perhaps the optical properties of an exogenous probe, model-based time-frequency analysis can increase performance.

Typically, there are two spectral modification processes: spectral absorption and spectral scattering. Both processes can be present in the tissue at the same time. Therefore, it is important for SOCT to separate the contributions from each of them. The number of the spectral bands analyzed by SOCT is often more than the number of spectral modification processes of interest; the separation is a mathematical overcomplete problem and can be obtained by spectral analysis. The first such attempt was through spectral triangulation,[53] which uses three probe lasers of equally spaced center wavelengths. Spectral triangulation was capable of separating the intrinsic first-order spectral scattering from the extrinsic dye absorption, and this technique was demonstrated with the use of ICG in a *Xenopus laevis* (African frog) tadpole (Fig. 13). A more sophisticated approach utilizes the least-squares fitting algorithms.[76] Compared to spectral triangulation, the least-squares fitting algorithm utilizes more frequency bands and is optimal for most practical problems.

In principle, SOCT can be used to map out absorbing probes or molecules such as Hb/HbO_2, melanin, and other endogenous chromophores. Among them, Hb/HbO_2 is especially interesting because of their abundance and their critically important role as indicators of tissue oxygenation states. Currently, two prominent methods for *in vivo* mapping of Hb/HbO_2 are functional magnetic resonance imaging (fMRI)[77] and NIR optical tomography.[78] However, fMRI suffers from low temporal resolution and NIR optical tomography suffers from low spatial resolution. SOCT theoretically can overcome both drawbacks with real-time OCT imaging with micrometer resolution. However, due to the time-frequency tradeoff problem mentioned before, the spatial resolution that can be achieved ultimately is dependent on the system sensitivity and noise reduction. In an early report, the oxygenation states of Hb/HbO_2 were distinguished by SOCT with 1-nm spectral resolution and 312-μm spatial resolution.[51] As a method for detecting and imaging not only endogenous molecular species but also exogenous probes, research in the use of SOCT will continue to define its applications and limitations.

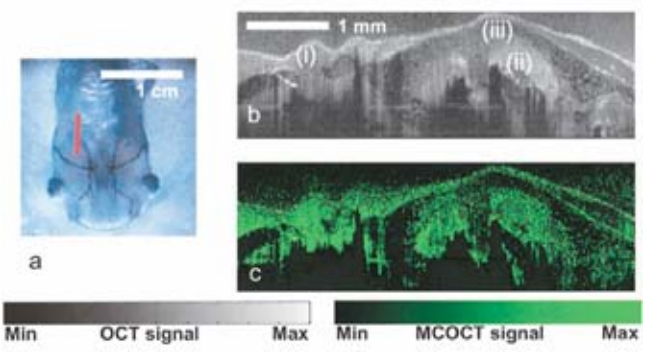

Fig. 13 Spectral triangulation. (a) Ventral view of a stage 54 *Xenopus laevis* tadpole. The line indicates the location where images were acquired. (b) OCT image of the region indicated in (a). (c) Spectral triangulation molecular-contrast OCT image from the same region. Legend: (i) parabranchial cavity, (ii) gill arches, and (iii) opercular field. Figure reprinted with permission.[53]

3.2 *Molecular Contrast through Nonlinear Interferometry*

Typical OCT methods measure the linear, elastic scattering of tissues, which are limited to the detection of scattering, absorption, spectral, and polarization properties inside the illumination bandwidth. Unfortunately, most molecules of interest do not have distinct scattering signatures in the near-infrared wavelengths commonly used in OCT. However, there are many nonlinear optical effects that biomolecules exhibit that can be used for molecular contrast. Nonlinear effects, including second harmonic generation (SHG)[79–83] and coherent anti-Stokes Raman scattering (CARS),[84–91] have recently been successfully integrated with OCT to produce images with endogenous molecular contrast.[92–95]

Unlike linear scattering, where individual photons independently scatter off of the sample, several photons mutually interact through the sample in nonlinear scattering processes. The incident photons are selected to promote a particular nonlinear process that produces molecular contrast. To interact at a particular point in the tissue, the interacting photons must, roughly speaking, arrive at the same place at the same time. Pulsed lasers are typically used to concentrate the photons into a small enough time interval, and focused beams are used to concentrate the photons into a small enough spatial extent, to produce a measurable nonlinear signal.

Only certain nonlinear processes are suited for nonlinear interferometry. The scattered radiation must remain coherent

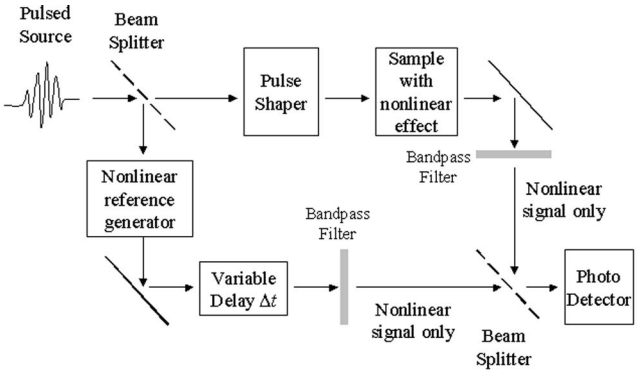

Fig. 14 Nonlinear interferometry concept for OCT. Schematic includes a broadband source, in which a portion of the source is also used to generate a reference pulse through a nonlinear optical method. A Mach-Zender interferometer configuration is shown, along with a pulse shaper in the sample arm to excite specific nonlinear effects in the sample. The detection scheme is simplified, and in practice a single-shot detection scheme using spectral-domain OCT techniques could be used. Modified figure reprinted with permission.[92]

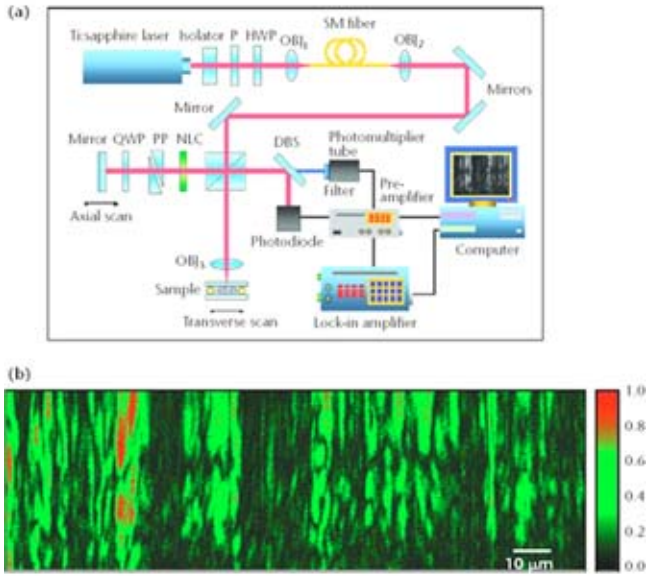

Fig. 15 Second harmonic OCT. (a) Experimental setup for performing SH-OCT. (b) 2-D high-resolution SH-OCT image acquired from a rat tail tendon. Abbreviations: DBS, dichroic beamsplitter; HWP, half-wave plate; P, polarizer; QWP, quarter-wave plate; NLC, nonlinear β-barium borate crystal; OBJ1-OBJ3, objectives; DBS, dichroic beamsplitter; PP, prism-pair dispersion compensator; and SM fiber, single-mode fiber. Modified figure reprinted with permission.[81]

with the illumination, which excludes effects such as spontaneous fluorescence and spontaneous Raman scattering. It is also desirable for the scattered radiation to be of a different frequency bandwidth than the incident radiation, so that the scattered radiation is easy to distinguish from the incident radiation. Because nonlinear processes are generally weak, any background signal can easily overwhelm the small nonlinear signal. Two nonlinear processes that satisfy the criteria for detection with nonlinear interferometry are SHG and CARS. Each of these processes provides differing information on the composition of tissue.

A representative schematic of how nonlinear interferometry can be integrated into OCT is shown in Fig. 14. A pulsed source produces the optical frequencies needed to stimulate the nonlinear process. This source is split between the two arms of an interferometer. In the sample arm, a pulse shaper is used to control the temporal profile of the pulse to excite a particular nonlinear process of interest. The shaped pulse is then focused into the sample, where the target molecular species will convert some of the radiation to a nonlinear signal. The backscattered signal from the sample is then filtered for the remaining excitation radiation. In the reference arm, a nonlinear reference generator, which can consist of the molecular species being imaged or a nonlinear crystal, converts some of the excitation wavelengths to the nonlinear band. The two nonlinear signals are combined with a beamsplitter, and the interference is measured as the relative time delay is scanned. The amplitude of the interference fringes indicates the density of the target molecular species.

Using interferometric detection of a nonlinear process itself has benefits over standard incoherent nonlinear microscopy such as SHG or CARS microscopy. OCT coherence gating can be performed on the returned nonlinear signal to range the depth of nonlinear scatterers in tissue. In nonlinear microscopy, the focus is scanned through the sample, because the nonlinear process itself limits the volume over which the interaction occurs. Interferometric detection also provides the heterodyne advantage, where the interference component of the signal may be increased until the signal-to-noise ratio is limited only by the available signal from the sample and not detector noise. Heterodyning also minimizes the noise caused by stray light. Finally, dual balancing or spectral interferometry can be used to minimize the effects of power fluctuations in the pulsed source.

Second harmonic generation is an effect where a nonlinear material will convert two photons of one frequency to a single photon of twice the frequency. Because of the symmetry of the process, SHG does not occur in a uniform, isotropic medium. SHG is generally produced at surfaces, in birefringent media, or by asymmetric structures such as rod-like or fiber-like structures. The SHG process can then better discriminate between uniform media, anisotropic structures produced by cell membranes, and commonly, collagen fibers. For example, SH-OCT has been proposed and demonstrated on collagen layers (Fig. 15).[81]

Another method of nonlinear contrast utilizes CARS, and is called nonlinear interferometric vibrational imaging (NIVI).[92] Raman scattering probes the vibrational resonance frequencies of molecules. Unlike other methods such as infrared spectroscopy, Raman scattering is a nonlinear process that can utilize wavelengths of 600 to 1500 nm in the biological window that are not absorbed by tissues. CARS is often used in microscopy instead of the more common spontaneous Raman scattering, because CARS produces a much stronger signal. Incoherent detection of CARS has been used in a manner analogous to two-photon microscopy to image biological tissues.[84–91] Using OCT optical ranging and interferometry techniques improves on these methods by taking advantage of the coherent nature of CARS, increasing the sensitivity, rejecting noise, and allowing the temporal ranging of the CARS signal.

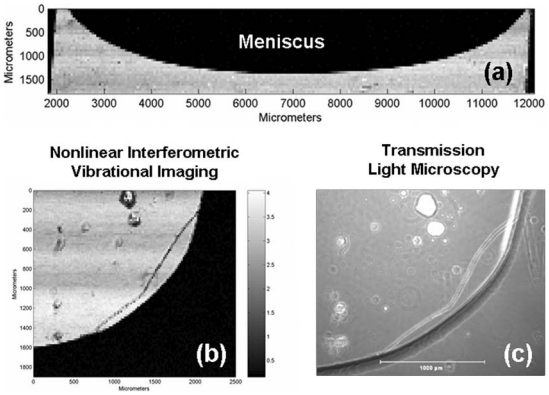

Fig. 16 Nonlinear interferometric vibrational imaging. NIVI images collected in transmission from various regions of a quartz cuvette filled with acetone. The NIVI system was tuned to a vibrational resonance of 2925 cm^{-1} corresponding to the C-H stretch of acetone. (a) Meniscus formed at the air-acetone surface inside the cuvette. (b) NIVI of the curved bottom of the cuvette. Signal is only produced from the acetone, not from the quartz wall, nor from air bubbles and contaminants. (c) Transmission light microscopy shows the visible optical transparency of both the acetone and the quartz, and strong correlation with the location and structural features of the contaminants.

The coherence gating and spatial localization of CARS signals has been demonstrated (Fig. 16), and is likely to provide an alternate method of locating molecular species in tissues.[93] In particular, NIVI[92] has been developed to allow the amplitude and phase of the nonlinear susceptibility to be inferred. This helps remove artifacts due to nonresonant processes that are not specific to the molecular frequencies of interest. These processes can dominate the nonlinear signal and therefore greatly reduce the molecular specificity of the method if they are not removed. The elimination of these nonresonant components was demonstrated[94] by coherence gating the CARS signal to exclude the nonresonant component. The interferometric reconstruction of the amplitude and phase of the Raman spectrum has been achieved[95] and has greatly increased confidence that further enhancements of the use of CARS in OCT will result in high fidelity images. As the techniques of ultrafast signal production and detection are refined, it seems likely that other coherent nonlinear processes will also be exploited to provide further molecular specificity.

4 Future Directions and Challenges

The recent advances and successes in the use of bioluminescent and targeted fluorescent probes have clearly established the use of optical molecular imaging for elucidating the pathogenesis of disease in preclinical animal models. Similarly, it is expected that advances in the development and use of molecular imaging probes for nonfluorescence- and nonbioluminescence-based optical imaging modalities such as OCT, light microscopy, and reflectance confocal microscopy will have an equally significant impact. Several active areas of research include targeting of probes, the development of externally and physiologically activatable probes, and the imaging of genetically engineered and expressed probes.

The ability to target molecular probes to site-specific cells or tissues not only has significant implications for enhancing image contrast and visualization, but also, and perhaps more importantly, enables the site-specific delivery of pharmacotherapeutics for treating the disease. Despite the advancements made in this area over decades of research, our ability to target a particular cell type with sufficient specificity remains relatively poor. However, there have been several commonly identified targets, including the folate receptor, which is expressed in normally low levels in adult tissues, but overexpressed in proliferating malignant cells,[96] and the sigma receptor, which can be highly overexpressed (up to ten-fold) in a variety of tumors including lung, renal, colon, central nervous system, breast, prostate, and melanoma.[97] Much of these limitations arise from our limited understanding of the molecular and cellular events occurring *in vivo* in these disease states, and the relatively small differences between target expression profiles on normal and abnormal cells. Given the intense scientific, medical, and economical incentives for advancing this research, our ability to target, image, and treat specific cells of interest will likely continue to improve over time.

The striking ability of optical techniques to image extremely weak optical signals is most appreciated with background rejection techniques, where the nonspecific optical signal is separable from the signal arising specifically from the contrast agents. Bioluminescence imaging is an excellent example, as are fluorescence-based confocal and multiphoton methods in the absence of autofluorescence. Of the methods and probes discussed in this work, the use of magnetomotive OCT and pump-probe OCT exhibit high degrees of background rejection, which can provide higher signal to noise than other techniques (such as those that rely simply on the addition of a strong scatterer or absorber to tissue). Classes of probes that would enable high specificity of detection are those that can be activated, either through some external trigger or internally, through some physiological process. The former method was demonstrated using a pump-probe OCT technique with probes that have varying absorption states.[55,56] The use of the latter method would enable a wide range of functional studies that could investigate physiological states and processes *in vivo* and in real time. While molecular beacons[98,99] and protease-activatable fluorescence probes[100] represent examples of this class of probes, the development of these physiologically activatable probes for OCT remains an active area of research.

Green fluorescent protein (GFP), its many variants, and other genetically encoded light-emitting proteins have expanded our ability to visualize biology in normal and diseased states.[101] It is also well recognized in the biomedical optics communities that there is a need for longer-wavelength probes in the near-infrared to reduce tissue damage and to increase imaging depth in highly scattering tissues. Recently, the DsRed protein, with longer-wavelength absorption and emission spectra, has been imaged using OCT in a pump-probe configuration.[102] This demonstration represents an important step in the use of genetically expressed probes in conjunction with OCT. Because of the imaging-depth penetration advantage that OCT provides over more traditional fluorescence-based microscopy methods, and the high spatial resolution advantage over bioluminescence-based imaging, the development of genetically expressed probes for OCT will likely expand the toolkit of investigational methods. Naturally occurring substances such as melanin, with its high refractive index

($n=1.7$), may offer another alternative.[103] In all of these cases, genetically expressing molecules that exhibit strong and modifiable scattering or absorbing properties detectable with molecular OCT techniques would further advance this field.

Recent advances in the development of molecular probes and techniques for OCT are accompanied with multiple challenges and limitations. Fundamental studies need to be completed that would fully characterize the optical properties of these probes in phantoms, cell culture, and in tissue, as well as under normal and pathologic conditions. Critical investigational studies are needed to determine the detection sensitivity and establish the limits to which these methods would be used for detecting at the cellular and molecular level, both in cell cultures and in animal models. As one would anticipate, higher concentrations of probes would generate stronger signals, yet careful *in vitro* and *in vivo* studies remain to be completed to determine the toxicity of these probes and the optical radiation used for their detection and imaging. To our advantage, many similar probes, such as albumin microspheres, iron oxides, absorbing molecules, and gold nanoparticles, are currently being used for molecular imaging techniques in other modalities including MRI and ultrasound. Additionally, many similar classes of probes suitable for use in OCT have been approved by the U.S. Federal Drug Administration such as Albunex®,[35] Feridex®,[104] and indocyanine green (ICG) dye,[105] to name a few. Finally, more quantitative studies are needed in normal and tumor animal models to both demonstrate the enhancement of contrast with these probes, and ultimately to show their use for improving our clinical diagnostic ability. Ideally, one would like to perform optical molecular imaging without the need of exogenous agents that could potentially induce toxicity or alter the physiology of the process one is wishing to measure. Optical methods, such as SOCT or NIVI, may in time be able to characterize the molecular composition of tissue with high sensitivity and specificity only by detecting variations from the incident optical radiation, and may ultimately prove to be most desirable.

While the development and experimental implementation of optical probes for OCT is still in its infancy, it is clear that the use of novel probes or contrast agents in OCT will enable OCT to progress to a new diagnostic level. Early applications of OCT focused on the morphological imaging capabilities of this technique. In recent years, attention has been given to the use of functional OCT techniques that provide additional information based on optical changes that correspond to physiological parameters. With the advent of molecular OCT imaging techniques, by use of exogenous probes or contrast agents, or by use of novel techniques to detect endogenous molecules, the imaging and diagnostic capabilities of OCT will be extended significantly. Ultimately, the task for the OCT community will be to demonstrate the clinical efficacy and improvement in diagnostic ability afforded by these emerging molecular OCT imaging techniques.

Acknowledgments

We wish to thank the members of the Biophotonics Imaging Laboratory at the Beckman Institute on the University of Illinois at Urbana-Champaign (UIUC) campus for their dedication and insight in this area of research. We also wish to thank our collaborators for their work in fabricating novel probes, including Kenneth Suslick, Department of Chemistry, UIUC, Kenneth Watkin, Department of Speech and Hearing Sciences, UIUC, and Alex Wei, Department of Chemistry, Purdue University, and appreciate the assistance of Janet Hanlon in preparing these figures. Finally, we thank our colleagues whose work is represented here for helping advance this field, and apologize to those whose work was not included due to space and depth of coverage constraints. This research was supported in part by The Whitaker Foundation (RG-01-0179, S.A.B.), the National Institutes of Health (NIBIB, 1 R01 EB-00-108, 1 R01 EB-03-003, S.A.B.), NCI/NASA (NAS2-02057, S.A.B.), and the Beckman Institute for Advanced Science and Technology. Additional information can be found at http://biophotonics.uiuc.edu.

References

1. S. Achilefu, R. B. Dorshow, J. E. Bugaj, R. Rajagopalan, "Novel receptor-targeted fluorescent contrast agents for *in vivo* tumor imaging," *Invest. Radiol.* **35**, 479–485 (2000).
2. R. Weissleder and V. Ntziachristos, "Shedding light onto live molecular targets," *Nat. Med.* **9**, 123–128 (2003).
3. S. Achilefu, "Lighting up tumors with receptor-specific optical molecular probes," *Technol. Cancer Res. Treat.* **3**, 393–409 (2004).
4. T. C. Doyle, S. M. Burns, and C. H. Contag, "*In vivo* bioluminescence imaging for integrated studies of infection," *Cell. Microbiol.* **6**, 303–317 (2004).
5. M. R. Hamblin, T. Zahra, C. H. Contag, A. T. McManus, and T. Hasan, "Optical monitoring and treatment of potentially lethal wound infections *in vivo*," *J. Infect. Dis.* **187**, 1717–1725 (2003).
6. S. Gross and D. Piwnica-Worms, "Spying on cancer: molecular imaging *in vivo* with genetically encoded reporters," *Cancer Cells* **7**, 5–15 (2005).
7. A. Rehemtulla, L. D. Stegman, S. J. Cardozo, S. Gupta, D. E. Hall, C. H. Contag, and B. D. Ross, "Rapid and quantitative assessment of cancer treatment response using *in vivo* bioluminescence imaging," *Neoplasia* **2**, 491–495 (2000).
8. X. Wang, M. Rosol, S. Ge, D. Peterson, G. McNamara, H. Pollack, D. B. Kohn, M. D. Nelson, and G. M. Crooks, "Dynamic tracking of human hematopoietic stem cell engraftment using *in vivo* bioluminescence imaging," *Blood* **102**, 3478–3482 (2003).
9. B. W. Rice, M. D. Cable, M. B. Nelson, "*In vivo* imaging of light-emitting probes," *J. Biomed. Opt.* **6**, 432–440 (2001).
10. J. E. Bugaj, S. Achilefu, R. B. Dorshow, and R. Rajagopalan, "Novel fluorescent contrast agents for optical imaging of *in vivo* tumors based on a receptor-targeted dye-peptide conjugate platform," *J. Biomed. Opt.* **6**(2), 122–133 (2001).
11. S. Stoyanov, "Probes: dyes fluorescing in the NIR region," in *Near-Infrared Applications in Biotechnology*, R. Raghavachari, Ed., pp. 35–93, Marcel Dekker, Inc., New York (2001).
12. D. Huang, E. A. Swanson, C. P. Lin, J. S. Schuman, W. G. Stinson, W. Chang, M. R. Hee, T. Flotte, K. Gregory, C. A. Puliafito, and J. G. Fujimoto, "Optical coherence tomography," *Science* **254**, 1178–1181 (1991).
13. *Handbook of Optical Coherence Tomography*, B. E. Bouma and G. J. Tearney, Eds., Marcel Dekker, Inc., New York (2001).
14. *Optical Coherence Tomography of Ocular Diseases*, J. S. Schuman, C. A. Puliafito, and J. G. Fujimoto, Eds., Slack, Inc., Thorofare, NJ (2004).
15. G. J. Tearney, M. E. Brezinski, B. E. Bouma, S. A. Boppart, C. Pitris, J. F. Southern, and J. G. Fujimoto, "*In vivo* endoscopic optical biopsy with optical coherence tomography," *Science* **276**, 2037–2039 (1997).
16. M. E. Brezinski, G. J. Tearney, B. E. Bouma, J. A. Izatt, M. R. Hee, E. A. Swanson, J. F. Southern, and J. G. Fujimoto, "Optical coherence tomography for optical biopsy: properties and demonstration of vascular pathology," *Circulation* **93**, 1206–1213 (1996).
17. S. A. Boppart, B. E. Bouma, C. Pitris, G. J. Tearney, J. F. Southern, M. E. Brezinski, and J. G. Fujimoto, "Intraoperative assessment of microsurgery with three-dimensional optical coherence tomography," *Radiology* **208**, 81–86 (1998).
18. Y. T. Pan, T. Q. Xie, C. W. Du, S. Bastacky, S. Meyers, and M. L.

Zeidel, "Enhancing early bladder cancer detection with fluorescence-guided endoscopic optical coherence tomography," *Opt. Lett.* **28**, 2485–2487 (2003).
19. I. K. Jang, G. J. Tearney, B. MacNeill, M. Takano, F. Moselewski, N. Ifitma, M. Shishkov, S. Houser, H. T. Aretz, E. F. Halpern, and B. E. Bouma, "*In vivo* characterization of coronary atherosclerosic plaque by use of optical coherence tomography," *Circulation* **111**, 1551–1555 (2005).
20. K. Bizheva, A. Unterhuber, B. Hermann, B. Povazay, H. Sattmann, A. F. Fercher, W. Drexler, M. Preusser, H. Budka, A. Stingl, and T. Le, "Imaging *ex vivo* healthy and pathologic human brain tissue with ultra-high-resolution optical coherence tomography," *J. Biomed. Opt.* **10**(1), 011006-1–7 (2005).
21. X. J. Wang, T. E. Milner, and J. S. Nelson, "Characterization of fluid flow velocity by optical Doppler tomography," *Opt. Lett.* **20**, 1337–1339 (1995).
22. Z. Chen, T. E. Milner, S. Srinivas, and X. Wang, "Noninvasive imaging of *in vivo* blood flow velocity using optical Doppler tomography," *Opt. Lett.* **22**, 1119–1121 (1997).
23. S. Yazdanfar, M. D. Kulkarni, and J. A. Izatt, "High resolution imaging of *in vivo* cardiac dynamics using color Doppler optical coherence tomography," *Opt. Express* **1**, 424–431 (1997).
24. J. K. Barton, J. A. Izatt, M. D. Kulkarni, S. Yazdanfar, and A. J. Welch, "Three-dimensional reconstruction of blood vessels from *in vivo* color Doppler optical coherence tomography images," *Dermatology (Basel, Switz.)* **198**, 355–361 (1999).
25. A. M. Rollins, S. Yazdanfar, J. K. Barton, and J. A. Izatt, "Real-time *in vivo* color Doppler optical coherence tomography," *J. Biomed. Opt.* **7**, 123–129 (2002).
26. J. F. de Boer, T. E. Milner, M. J. C. van Gemert, and J. S. Nelson, "Two-dimensional birefringence imaging in biological tissue by polarization-sensitive optical coherence tomography," *Opt. Lett.* **22**, 934–936 (1997).
27. M. J. Everett, K. Schoenenberger, B. W. Colston, Jr., and L. B. Da Silva, "Birefringence characterization of biological tissue by use of optical coherence tomography," *Opt. Lett.* **23**, 228–230 (1998).
28. S. Jiao and L. V. Wang, "Two-dimensional depth-resolved Mueller matrix of biological tissue measured with double-beam polarization-sensitive optical coherence tomography," *Opt. Lett.* **27**, 101–103 (2002).
29. J. F. de Boer and T. E. Milner, "Review of polarization sensitive optical coherence tomography and Stokes vector determination," *J. Biomed. Opt.* **7**(3), 359–371 (2002).
30. R. Uma Maheswari, H. Takaoka, R. Homma, H. Kadono, and M. Tanifuji, "Implementation of optical coherence tomography (OCT) in visualization of functional structures of cat visual cortex," *Opt. Commun.* **202**, 47–54 (2002).
31. M. Lazebnik, D. L. Marks, K. Potgieter, R. Gillette, and S. A. Boppart, "Functional optical coherence tomography for detecting neural activity through scattering changes," *Opt. Lett.* **28**, 1218–1220 (2003).
32. K. Bizheva, R. Pflug, B. Hermann, B. Povay, S. Gasparoni, H. Sattmann, A. Unterhuber, E. M. Anger, H. Reitsamer, S. Popov, J. R. Tylor, V. P. Gapontsev, P. Ahnelt, and W. Drexler, "Noninvasive spatially resolved probing of retinal physiology with functional ultrahigh resolution optical coherence tomography," presented at Coherence Domain Optical Methods and Optical Coherence Tomography in Biomedicine IX, 23 January 2005, San Jose, CA, Paper 5690-67, SPIE.
33. C. Yang, "Molecular contrast optical coherence tomography: a review," *Photochem. Photobiol.* **81**, 215–237 (2005).
34. M. Horisberger, "Colloidal gold: a cytochemical marker for light and fluorescent microscopy and for transmission and scanning electron microscopy," *Scan Electron Microsc.* **11**, 9–31 (1981).
35. C. Christiansen, H. Kryvi, P. C. Sontum, and T. Skotland, "Physical and biochemical characterization of Albunex, a new ultrasound contrast agent consisting of air-filled albumin microspheres suspended in a solution of human albumin," *Biotechnol. Appl. Biochem.* **19**, 307–320 (1994).
36. J. K. Barton, J. B. Hoying, and C. J. Sullivan, "Use of microbubbles as an optical coherence tomography contrast agent," *Acad. Radiol.* **9S**, 52–55 (2002).
37. T. M. Lee, A. L. Oldenburg, S. Sitafalwalla, D. L. Marks, W. Luo, F. Jean-Jacques Toublan, K. S. Suslick, and S. A. Boppart, "Engineered microsphere contrast agents for optical coherence tomography," *Opt. Lett.* **28**, 1546–1548 (2003).
38. J. R. Gunther, A. L. Oldenburg, and S. A. Boppart, "Macrophage viability following exposure and imaging of optical coherence tomography protein microsphere contrast agents," unpublished data (2005).
39. A. L. Klibanov, "Targeted delivery of gas-filled microspheres, contrast agents for ultrasound imaging," *Adv. Drug Delivery Rev.* **37**, 139–157 (1999).
40. K. Sokolov, M. Follen, J. Aaron, I. Pavlova, A. Malpica, R. Lotan, and R. Richards-Kortum, "Real-time vital optical imaging of precancer using anti-epidermal growth factor receptor antibodies conjugated to gold nanoparticles," *Cancer Res.* **63**, 1999–2004 (2003).
41. K. Sokolov, J. Aaron, B. Hsu, D. Nida, A. Gillenwater, M. Follen, C. MacAulay, K. Adler-Storthz, B. Korgel, M. Descour, R. Pasqualini, W. Arap, W. Lam, and R. Richards-Kortum, "Optical systems for *in vivo* molecular imaging of cancer," *Technol. Cancer Res. Treat.* **2**, 491–504 (2003).
42. J. N. Anker and R. Kopelman, "Magnetically modulated optical nanoprobes," *Appl. Phys. Lett.* **82**, 1102–1104 (2003).
43. *Scientific and Clinical Applications of Magnetic Carriers*, U. Hafeli, W. Schutt, J. Teller, and M. Zborowski, Eds., Plenum Press, New York (1997).
44. A. L. Oldenburg, J. R. Gunther, F. Jean-Jacques Toublan, D. L. Marks, K. S. Suslick, and S. A. Boppart, "Magnetic contrast agents for optical coherence tomography," *Proc. SPIE* **5316**, 91–98 (2004).
45. A. L. Oldenburg, J. R. Gunther, F. Jean-Jacques Toublan, D. L. Marks, K. S. Suslick, and S. A. Boppart, "Selective OCT imaging of cells using magnetically-modulated optical contrast agents," *Proc. Conf. Lasers Electro-Optics*, Optical Society of America, Washington, DC, pp. 405–406 (2003).
46. A. L. Oldenburg, J. R. Gunther, and S. A. Boppart, "Imaging magnetically labeled cells with magnetomotive optical coherence tomography," *Opt. Lett.* **30**, 747–749 (2005).
47. S. Hamaguchi, I. Tohnai, A. Ito, K. Mitsudo, T. Shigetomi, M. Ito, H. Honda, T. Kobayashi, and M. Ueda, "Selective hyperthermia using magnetoliposomes to target cervical lymph node metastasis in a rabbit tongue tumor model," *Cancer Sci.* **94**, 834–839 (2003).
48. E. Romanus, M. Huckel, C. Gross, S. Prass, W. Weitschies, R. Brauer, and P. Weber, "Magnetic nanoparticle relaxation measurement as a novel tool for *in vivo* diagnostics," *J. Magn. Magn. Mater.* **252**, 387–389 (2002).
49. A. S. Lubbe, C. Alexiou, and C. Bergemann, "Clinical applications of magnetic drug targeting," *J. Surg. Res.* **95**, 200–206 (2001).
50. A. H. Schmieder, P. M. Winter, S. D. Caruthers, T. D. Harris, T. A. Williams, J. S. Allen, E. K. Lacy, H. Zhang, M. J. Scott, G. Hu, J. D. Robertson, S. A. Wickline, and G. M. Lanza, "Molecular MR imaging of melanoma angiogenesis with $\alpha_v\beta_3$-targeted paramagnetic nanoparticles," *Magn. Reson. Med.* **53**, 621–627 (2005).
51. D. J. Faber, E. G. Mik, M. C. G. Aalders, and T. G. van Leeuwen, "Light absorption of (oxy-)hemoglobin assessed by spectroscopic optical coherence tomography," *Opt. Lett.* **28**, 1436–1438 (2003).
52. T. Stren, A. Simonsen, O. J. Lkberg, T. Lindmo, L. O. Svaasand, and A. Ryset, "Measurement of dye diffusion in agar by use of low-coherence interferometry," *Opt. Lett.* **28**, 1215–1217 (2003).
53. C. Yang, L. E. McGuckin, J. D. Simon, M. A. Choma, B. E. Applegate, and J. A. Izatt, "Spectral triangulation molecular contrast optical coherence tomography with indocyanine green as the contrast agent," *Opt. Lett.* **29**, 2016–2018 (2004).
54. C. Xu, J. Ye, D. L. Marks, and S. A. Boppart, "Near-infrared dyes as contrast-enhancing agents for spectroscopic optical coherence tomography," *Opt. Lett.* **29**, 1647–1649 (2004).
55. K. D. Rao, M. A. Choma, S. Yazdanfar, A. M. Rollins, and J. A. Izatt, "Molecular contrast in optical coherence tomography by use of a pump-probe technique," *Opt. Lett.* **28**, 340–342 (2003).
56. C. Yang, M. A. Choma, L. E. Lamb, J. D. Simon, and J. A. Izatt, "Protein-based molecular contrast optical coherence tomography with phytochrome as the contrast agent," *Opt. Lett.* **29**, 1396–1398 (2004).
57. A. Wei, "Plasmonic nanomaterials," in *Nanoparticles: Scaffolds and Building Blocks*, V. M. Rotello, Ed., pp. 173–200, Kluwer Academic, New York (2003).
58. J. Yguerabide and E. E. Yguerabide, "Light-scattering submicroscopic particles as highly fluorescent analogs and their use as tracer labels in clinical and biological applications: I. Theory," *Anal. Biochem.* **262**, 137–156 (1998).
59. C. Loo, A. Lin, L. Hirsch, M. H. Lee, J. Barton, N. Halas, J. West, and R. Drezek, "Nanoshell-enabled photonics-based imaging and

therapy of cancer," *Technol. Cancer Res. Treat.* **3**, 33–40 (2004).
60. A. L. Oldenburg, D. A. Zweifel, C. Xu, A. Wei, and S. A. Boppart, "Characterization of plasmon-resonant gold nanorods as near-infrared optical contrast agents investigated using a double-integrating sphere system," *Proc. SPIE* **5703**, 50–60 (2005).
61. J. Chen, F. Saeki, B. J. Wiley, H. Cang, M. J. Cobb, Z. Y. Li, L. Au, H. Zhang, M. B. Kimmey, X. Li, and Y. Xia, "Gold nanocages: bioconjugation and their potential use as optical imaging contrast agents," *Nano Lett.* **5**, 473–477 (2005).
62. K. Chen, Y. Liu, G. Ameer, and V. Backman, "Optimal design of structured nanospheres for ultrasharp light-scattering resonances as molecular imaging multilabels," *J. Biomed. Opt.* **10**, 024005 (2005).
63. S. L. Westcott, J. B. Jackson, C. Radloff, and N. J. Halas, "Relative contributions to the plasmon line shape of metal nanoshells," *Phys. Rev. B* **66**, 155431-1–5 (2002).
64. T. S. Tkaczyk, M. Rahman, V. Mack, K. Sokolov, J. D. Rogers, R. Richards-Kortum, and M. R. Descour, "High resolution, molecular-specific, reflectance imaging in optically dense tissue phantoms with structure-illumination," *Opt. Express* **12**, 3745–3758 (2004).
65. J. B. Jackson, S. L. Westcoot, L. R. Hirsch, J. L. West, and N. J. Halas, "Controlling the surface enhanced Raman effect via the nanoshell geometry," *Appl. Phys. Lett.* **82**, 257–259 (2003).
66. R. D. Averitt, S. L. Westcoot, and N. J. Halas, "Linear optical properties of gold nanoshells," *J. Opt. Soc. Am. B* **16**, 1824–1832 (1999).
67. L. R. Hirsch, R. J. Stafford, J. A. Bankson, S. R. Sershen, B. Rivera, R. E. Price, J. D. Hazle, N. J. Halas, and J. L. West, "Nanoshell-mediated near-infrared thermal therapy of tumors under magnetic resonance guidance," *Proc. Natl. Acad. Sci. U.S.A.* **100**, 13549–13554 (2003).
68. S. Link, M. B. Mohamed, and M. A. El-Sayed, "Simulation of the optical absorption spectra of gold nanorods as a function of their aspect ratio and the effect of the medium dielectric constant," *J. Phys. Chem. B* **103**, 3073–3077 (1999).
69. C. Sonnichsen, T. Franzl, T. Wilk, G. von Plessen, and J. Feldmann, "Drastic reduction of plasmon damping in gold nanorods," *Phys. Rev. Lett.* **88**, 077402-1–3 (2002).
70. U. Morgner, W. Drexler, F. C. Kartner, X. D. Li, C. Pitris, E. P. Ippen, and J. G. Fujimoto, "Spectroscopic optical coherence tomography," *Opt. Lett.* **25**, 111–113 (2000).
71. R. Leitgeb, M. Wojtkowski, A. Kowalczyk, C. K. Hitzenberger, M. Sticker, and A. F. Fercher, "Spectral measurement of absorption by spectroscopic frequency-domain optical coherence tomography," *Opt. Lett.* **25**, 820–822 (2000).
72. B. Hermann, K. Bizheva, A. Unterhuber, B. Povazay, H. Sattmann, L. Schmetterer, A. F. Fercher, and W. Drexler, "Precision of extracting absorption profiles from weakly scattering media with spectroscopic time-domain optical coherence tomography," *Opt. Express* **12**, 1677–1688 (2004).
73. C. Xu, F. Kamalabadi, and S. A. Boppart, "Comparative performance analysis of time-frequency distributions for spectroscopic optical coherence tomography," *Appl. Opt.* **44**, 1813–1822 (2005).
74. *Practical Time-Frequency Analysis*, R. Carmona, W. Hwang, and B. Torresani, Eds., Academic Press, San Diego, CA (1998).
75. L. Cohen, "Time-frequency distributions—a review," *Proc. IEEE* **77**, 941–981 (1989).
76. C. Xu, D. L. Marks, M. N. Do, and S. A. Boppart, "Separation of absorption and scattering profiles in spectroscopic optical coherence tomography using a least-squares algorithm," *Opt. Express* **12**, 4790–4803 (2004).
77. H. Bruhn, P. Fransson, and J. Frahm, "Modulation of cerebral blood oxygenation by indomethacin: MRI at rest and functional brain activation," *J. Magn. Reson Imaging* **13**, 325–334 (2001).
78. B. Chance, "Near-infrared images using continuous, phase-modulated, and pulsed light with quantitation of blood and blood oxygenation," *Ann. N.Y. Acad. Sci.* **838**, 29–45 (1998).
79. Y. Jiang, I. Tomov, Y. Wang, and Z. Chen, "Second-harmonic optical coherence tomography," *Opt. Lett.* **29**, 1090–1092 (2004).
80. C. Vinegoni, J. S. Bredfeldt, D. L. Marks, and S. A. Boppart, "Nonlinear optical contrast enhancement for optical coherence tomography," *Opt. Express* **12**, 331–341 (2004).
81. Y. Jiang, I. Tomov, Y. Wang, and Z. Chen, "High resolution second harmonic optical coherence tomography," *Opt. Photonics News* **15**, 22 (2004).
82. B. E. Applegate, C. Yang, A. M. Rollins, and J. A. Izatt, "Polarization-resolved second-harmonic-generation optical coherence tomography in collagen," *Opt. Lett.* **29**, 2252–2254 (2004).
83. S. Yazdanfar, L. H. Laiho, and P. T. C. So, "Interferometric second harmonic generation microscopy," *Opt. Express* **12**, 2739–2745 (2004).
84. M. D. Duncan, J. Reintjes, and T. J. Mannucia, "Scanning coherent anti-Stokes Raman microscope," *Opt. Lett.* **7**, 350–352 (1982).
85. A. Zumbusch, G. R. Holtom, and X. S. Xie, "Three-dimensional vibrational imaging by coherent anti-Stokes Raman scattering," *Phys. Rev. Lett.* **82**, 4142–4145 (1999).
86. E. O. Potma, D. J. Jones, J. X. Cheng, X. S. Xie, and J. Ye, "High sensitivity coherent anti-Stokes Raman scattering microscopy with two tightly synchronized picosecond lasers," *Opt. Lett.* **27**, 1168–1170 (2002).
87. J.-X. Cheng, A. Volkmer, L. D. Book, and X. S. Xie, "An epi-detected anti-Stokes Raman scattering (E-CARS) microscope with high spectral resolution and high sensitivity," *J. Phys. Chem. B* **105**, 1277–1280 (2001).
88. J.-X. Cheng, L. D. Book, and X. S. Xie, "Polarization coherent anti-Stokes Raman scattering microscopy," *Opt. Lett.* **26**, 1341–1343 (2001).
89. N. Dudovich, D. Oron, and Y. Silberberg, "Single-pulse coherent controlled nonlinear Raman spectroscopy and microscopy," *Nature (London)* **418**, 512–514 (2002).
90. G. W. H. Wurpel, J. M. Schins, and M. Muller, "Direct measurement of chain order in single phospholipid mono- and bilayers with multiplex CARS," *J. Phys. Chem. B* **108**, 3400–3403 (2004).
91. K. P. Knutsen, J. C. Johnson, A. E. Miller, P. B. Petersen, and R. J. Saykally, "High spectral resolution multiplex CARS microscopy using chirped pulses," *Chem. Phys. Lett.* **387**, 436–441 (2004).
92. D. L. Marks and S. A. Boppart, "Nonlinear interferometric vibrational imaging," *Phys. Rev. Lett.* **92**, 123905-1–4 (2004).
93. J. S. Bredfeldt, C. Vinegoni, D. L. Marks, and S. A. Boppart, "Molecularly sensitive optical coherence tomography," *Opt. Lett.* **30**, 495–497 (2005).
94. D. L. Marks, C. Vinegoni, J. S. Bredfeldt, and S. A. Boppart, "Interferometric differentiation between resonant coherent anti-Stokes Raman scattering and nonresonant four-wave-mixing processes," *Appl. Phys. Lett.* **85**, 5787–5789 (2004).
95. C. L. Evans, E. O. Potma, and X. S. Xie, "Coherent anti-Stokes Raman scattering spectral interferometry: determination of the real and imaginary components of nonlinear susceptibility chi(3) for vibrational microscopy," *Opt. Lett.* **29**, 2923–2925 (2004).
96. Y. Lu, E. Sega, C. P. Leamon, and P. S. Low, "Folate receptor-targeted immunotherapy of cancer: mechanism and therapeutic potential," *Adv. Drug Delivery Rev.* **56**, 1161–1176 (2004).
97. K. T. Wheeler, L. M. Wang, C. A. Wallen, S. R. Childers, J. M. Cline, P. C. Keng, and R. H. Mach, "Sigma-2 receptors as a biomarker of proliferation in solid tumours," *Br. J. Cancer* **82**, 1223–1232 (2000).
98. C. Xi, M. Balberg, S. A. Boppart, and L. Raskin, "Use of DNA and peptide nucleic acid (PNA) molecular beacons for the detection and quantification of rRNA in solutions and in whole cells," *Appl. Environ. Microbiol.* **69**, 5673–5678 (2003).
99. X. H. Peng, Z. H. Cao, J. T. Xia, G. W. Carlson, M. M. Lewis, W. C. Wood, and L. Yang, "Real-time detection of gene expression in cancer cells using molecular beacon imaging: new strategies for cancer research," *Cancer Res.* **65**, 1909–1917 (2005).
100. C. H. Tung, Q. Zeng, K. Shah, D. E. Kim, D. Schellingerhout, and R. Weissleder, "*In vivo* imaging of beta-galactosidase activity using far red fluorescent switch," *Cancer Res.* **64**, 1579–1583 (2004).
101. J. Haseloff, E. L. Dormand, and A. H. Brand, "Live imaging with green fluorescent protein," *Methods Mol. Biol.* **122**, 241–259 (1999).
102. B. E. Applegate, M. V. Sarunik, C. Yang, and J. A. Izatt, "Molecular contrast optical coherence tomography: SNR comparison of techniques and introduction of ground state recovery pump-probe OCT," *Proc. SPIE* **5690**, 182–186 (2005).
103. A. Vitkin, J. Woolsey, B. C. Wilson, and R. R. Anderson, "Optical and thermal characterization of natural (*sepia officinalis*) melanin," *Photochem. Photobiol.* **59**, 455–462 (1994).
104. O. Clement, N. Siauve, C. A. Cuenod, and G. Frija, "Liver imaging with ferumoxides (Feridex): fundamentals, controversies, and practical aspects," *Top Magn. Reson Imaging* **9**, 167–182 (1998).
105. S. L. Owens, "Intravenous and indocyanine green angiography," *Br. J. Ophthamol.* **75**, 743–755 (2004).